

Coevolution of Iron, Phosphorus, and Sulfur Speciation during Anaerobic Digestion with Hydrothermal Pretreatment of Sewage Sludge

Qian Wang, Chiqian Zhang, Dhara Patel, Haesung Jung, Pan Liu, Biao Wan, Spyros G. Pavlostathis, and Yuanzhi Tang*



Cite This: *Environ. Sci. Technol.* 2020, 54, 8362–8372



Read Online

ACCESS |



Metrics & More

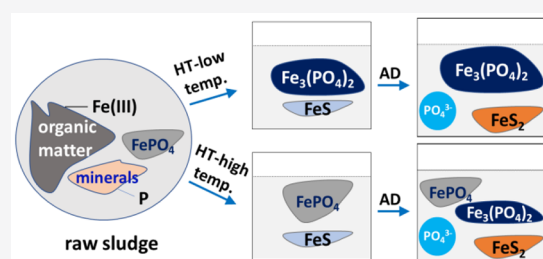


Article Recommendations



Supporting Information

ABSTRACT: Anaerobic digestion (AD) with hydrothermal (HT) pretreatment is an emerging technology for enhanced resource recovery from sewage sludge. This study investigates the speciation of Fe, P, and S during sequential HT–AD treatment of sewage sludge using sequential chemical extraction, X-ray diffraction, and X-ray absorption spectroscopy. Results suggest strong correlations between Fe and P species as well as Fe and S species, affecting the solubility and bioavailability of each other. For instance, much vivianite formed in the hydrochars after HT treatment at low temperature, while more strengite precipitated at higher HT temperature. During the subsequent AD process, microbial reduction of strengite and other Fe(III) species led to the formation of more vivianite, with concurrent P release into the solution and adsorption onto other minerals. HT pretreatment of sewage sludge had a weak effect on the sulfidation of Fe during the AD process. This work has important implications for understanding the nutrient speciation and availability in sludge-derived hydrochars and AD solids. It also provides fundamental knowledge for the selection and optimization of HT pretreatment conditions for enhanced resource recovery through sequential HT–AD process.



1. INTRODUCTION

Water resource recovery facilities (WRRFs) widely employ the activated sludge process to treat municipal wastewater, which generates tremendous amounts of municipal sewage sludge as a byproduct.¹ Sewage sludge typically contains high levels of recalcitrant organic matter, heavy metals, pesticides, herbicides, and water-borne pathogens, making its utilization, downstream treatment, and/or final disposal challenging and costly.^{2,3} On the other hand, sewage sludge has high contents of organic matter and nutrients (e.g., phosphorus, P, and nitrogen, N), serving as a promising candidate for energy recovery via biogas production and nutrient recycling/reclamation.²

Anaerobic digestion (AD) with hydrothermal (HT) pretreatment (i.e., sequential HT–AD treatment) is an emerging technology for sludge management and resource recovery.^{4–7} AD is a traditional biological process to degrade organic matter and recover energy from sewage sludge. During AD, fermentative and anaerobic microbes convert organic matter to biogas (biomethane and carbon dioxide). HT is a thermochemical conversion process, and low temperature HT pretreatment has been shown to improve sludge dewaterability, organic degradation, and biogas production during the subsequent AD.^{5–7} HT pretreatment can also provide a heated feedstock stream for AD,⁸ which typically needs to be maintained at 35 °C.

Both HT and AD can significantly affect the speciation of elements such as carbon (C), nutrients (P, N), and heavy metals, thus affecting their fate, mobility, and bioavailability. Meanwhile, the speciation of redox-sensitive elements such as iron (Fe) and sulfur (S) can also exert important controls on the chemical environment and mineral states of nutrients and metals. For example, HT treatment of biosolids was shown to convert organic phosphate into inorganic orthophosphate in the produced hydrochars.^{2,9} The final P speciation is closely related to the composition/speciation of metals and their affinities for P,¹⁰ HT temperature and duration, the source of biosolids, and pH.^{2,9,11} S in sewage sludge can react with metals to form metal sulfides via hydrothermal sulfidation.^{12–14} HT of sewage sludge under acidic and neutral environments also creates reducing chemical environments, where organic matter can reduce Fe(III) to Fe(II) species,^{15–17} such as the conversion of Fe₂O₃ to magnetite.¹⁷

Received: January 24, 2020

Revised: March 26, 2020

Accepted: June 15, 2020

Published: June 15, 2020



Studies have also investigated elemental speciation during AD. For instance, almost all of the P in anaerobically digested sludge is inorganic orthophosphate.¹⁸ All Fe(III) was reduced to Fe(II) after long-term AD.¹⁹ In the presence of Fe, vivianite ($\text{Fe}_3(\text{PO}_4)_2 \cdot 8\text{H}_2\text{O}$) is the dominant phosphate mineral in anaerobically digested sludge at pH 7–9 under low oxidation–reduction potential (ORP) conditions.^{3,20} The frequent occurrence of vivianite precipitation²¹ and its easy separation under a magnetic field makes it a promising means to recover P.²² During AD, sulfate can be reduced to sulfides,^{23,24} and hydrogen sulfide is generated from sludges with high S content, affecting biogas production.²⁵ Sulfate reduction also facilitates phosphate release to the aqueous phase during AD.²⁶

A considerable number of studies have investigated elemental speciation during separate HT and AD processes. However, speciation transformation on nutrients and metals during sequential HT–AD is lacking. Our recent work investigated the energy (i.e., methane) and nutrient (i.e., P) recovery from sewage sludge and manure during the sequential HT–AD process.²⁷ However, the correlation between P speciation and other redox-sensitive elements such as Fe and S during the combined HT–AD process has not been clarified, despite the previously observed strong correlation between Fe chemistry and P recovery from sewage sludge,²⁸ as well as the influence of S on Fe chemistry as a redox couple that strongly affects the chemical environment during treatment processes.²⁹ During HT pretreatment, the rate of organic matter hydrolysis is mainly determined by the treatment temperature. HT below 190 °C can serve as a pretreatment step to enhance biogas production during AD,³⁰ whereas HT at higher temperature reduces organic matter degradability due to the production of toxic/inhibitory intermediates.³¹ Therefore, in this study, the HT pretreatment was conducted at 90, 155, and 185 °C, representing different hydrothermal conditions. The subsequent AD of hydrothermally treated sludge lasted 79 days. Complementary sequential chemical extraction, X-ray diffraction (XRD), and X-ray absorption spectroscopy (XAS) analyses were conducted to systematically characterize the speciation, mineralogy, and mobility of P and the important redox-sensitive elements Fe and S in HT-derived hydrochars and AD final solids during the sequential HT–AD process.

2. MATERIALS AND METHODS

2.1. Sample Collection. Sewage sludge and secondary wastewater effluent samples were collected from the F. Wayne Hill Water Resources Center (Buford, GA, USA). The Center mixes primary and waste-activated sludge, removes internal P for P release, and thickens the sludge before the on-site AD (see Figure S1 for the schematic process diagram of this center). The sludge mixture used in this study is the thickened sludge before it enters the plant anaerobic digesters. The sludge mixture has a total solids (TS) concentration of approximately 60 g/L and is a blend of primary and waste-activated sludge at a TS mass ratio of 63:37. The water content of the sludge mixture is 94 wt %. Table S1 shows the concentrations of major metals in the dry sludge mixture. The secondary wastewater effluent was used to prepare the AD matrix. The sludge mixture and secondary wastewater effluent were stored in the dark at 4 °C without any pretreatment for less than 3 days before the HT–AD treatment. Digestate from the anaerobic digester in the Center was also collected. After anaerobic incubation in the lab at 35 °C until production of

biogas was negligible, the digestate served as the inoculum for AD.

2.2. HT and AD Experiments. For HT at each temperature, 130 mL of sludge mixture was added to a 200 mL polypropylene-lined stainless steel hydrothermal reactor (COL-INT Tech., SC, USA). The reactor was sealed and heated in an oven at 90, 155, or 185 °C for 4 h (3 h ramping and 1 h holding time at the target temperature) and then allowed to cool down to room temperature in the air. Six replicates were processed for each HT temperature. After HT, the produced slurries were stored in glass bottles in the dark at 4 °C before subsequent AD. Aliquots of the sludge mixture and HT slurries were centrifuged to separate the solids (hydrochars hereinafter, although HT at 90 °C did not readily convert biomass to chars) and supernatant (HT process water hereinafter). The hydrochars were freeze dried until no further weight loss before composition analysis.

Subsequent AD experiments were conducted in 600 mL glass reactors. Calculated amount of the HT-derived slurries (i.e., hydrochar and HT process water at 2 g volatile solids (VS)/L final concentration), sodium bicarbonate (1.4 g/L, final concentration), and anaerobic inoculum (2 g VS/L, final concentration) were added to each AD reactor. For each reactor, the initial volume of the anaerobic matrix was brought to 400 mL by adding the secondary wastewater effluent. No artificial medium was added. The reactors were then capped with rubber stoppers and anaerobically digested for 79 days at 35 °C while being shaken at ~220 rpm. Two controls were also set up: one with the raw sludge mixture without HT (AD control), and the second with the anaerobic inoculum without the sludge mixture (inoculum control).

During AD, biogas production and composition were monitored periodically. At the end of the anaerobic operation, a portion of the liquid content from each AD reactor (including the controls) was transferred to an anaerobic chamber (95% N_2 and 5% H_2 ; COY Lab), where the solids (AD solids hereinafter) and liquid (AD process water hereinafter) were separated using 0.45 μm membrane filters. The obtained AD solids were air dried for composition analysis as described below. The treatment conditions and sample labels are given in Table 1.

2.3. Characterization of Raw Sludge, Hydrochars, and AD Solids. Composition analysis was conducted using inductively coupled plasma optical emission spectrometry (ICP-OES) on aqua regia digested solids (raw sludge mixture,

Table 1. Treatment Conditions and Sample Labels for HT- and AD-Treated Samples

Sample Label	Reaction Condition ^a
SWE	secondary wastewater effluent, pH 7.26
AI1	anaerobic inoculum before AD, pH 8.14
AI2	anaerobic inoculum after 79 days AD, pH 7.96
raw sludge	raw sludge mixture, pH 6.34
AD alone	AD of raw sludge, 35 °C, 79 days, pH 7.69
HT90	HT of raw sludge, 90 °C, 4 h, pH 6.04
HT90-AD	AD of HT90-derived slurries, 35 °C, 79 days, pH 7.49
HT155	HT of raw sludge, 155 °C, 4 h, pH 5.67
HT155-AD	AD of HT155-derived slurries, 35 °C, 79 days, pH 7.47
HT185	HT of raw sludge, 185 °C, 4 h, pH 5.41
HT185-AD	AD of HT185-derived slurries, 35 °C, 79 days, pH 7.46

^apH values were measured at the end of HT and AD treatments.

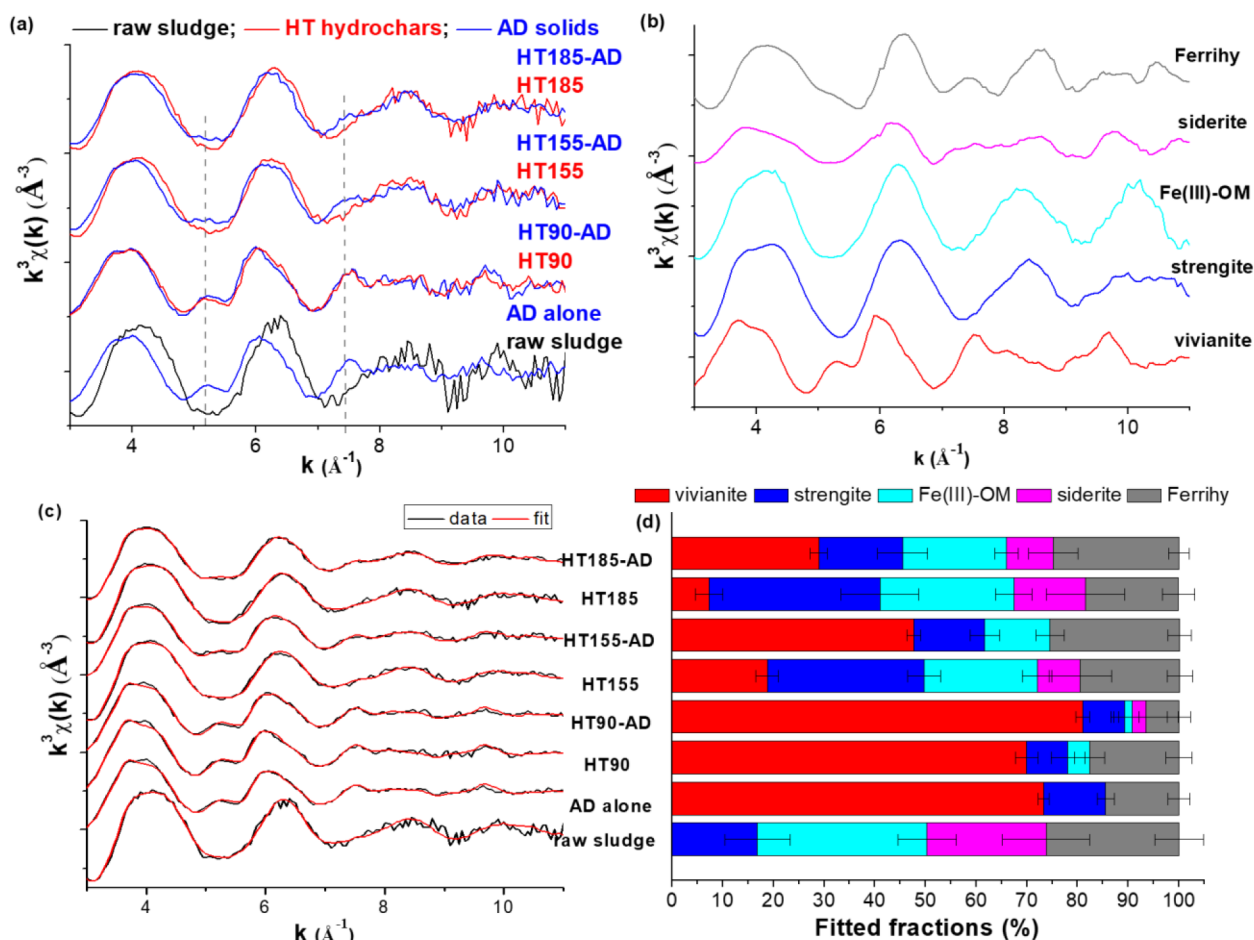


Figure 1. Fe K-edge k^3 -weighted EXAFS results. (a) EXAFS spectra of raw sludge, AD-alone solid, HT hydrochars, and AD solids after HT treatment at 90, 155, or 185 °C. (b) EXAFS spectra of reference compounds used for linear combination fitting (LCF) analyses, including vivianite, strengite, Fe(III)-organic complex (Fe(III)-OM), siderite, and ferrihydrite (Ferrihy). (c) Raw and fitted spectra. (d) Relative percentage of contributing Fe species determined by LCF.

hydrochars, and AD solids) and 0.45 μm membrane filtered liquids (the secondary wastewater effluent, HT process water, and AD process water). Fe, P, and S K-edge X-ray absorption spectroscopy (XAS) analyses, X-ray diffraction (XRD), and X-ray photoelectron spectroscopy (XPS) were conducted on the raw sludge, hydrochars, and AD solids. The Supporting Information (SI) Text S1 details the data collection procedure for Fe K-edge extended X-ray absorption fine structure (EXAFS) and P and S K-edge X-ray absorption near-edge structure (XANES), XRD, and XPS.

XAS data analysis was performed with the Athena software.³² Principal component analysis (PCA), target transformation (TT), and linear combination fitting (LCF) were performed on sample spectra to determine the number, identity, and contribution of end member phases. LCF of Fe EXAFS was conducted in the k^3 -weighted χ space (3–11.5 Å⁻¹) using a library of Fe reference compounds. LCF analyses of P and S XANES data was conducted at an energy range from –20 to +60 eV relative to the edge energy. The goodness of LCF was evaluated using the R factor, and the fits with the smallest R factors were reported.

Representative sets of Fe, P, and S reference compounds were used for LCF analysis. Fe reference compounds include iron sulfide, ferrihydrite, goethite, hematite, lepidocrocite, magnetite, siderite, carbonated green rust, sulfated green rust,

vivianite,³³ strengite,^{34,35} and Fe(III)-organic complex (Fe(III)-OM).³⁶ P reference compounds include Fe-associated P (vivianite,³⁷ $\text{FePO}_4 \cdot 2\text{H}_2\text{O}$, and phosphate sorbed on ferrihydrite), Al-associated P (AlPO_4 and phosphate sorbed on γ -alumina), Ca-associated P (octacalcium phosphate, OctaCa,¹⁰ and hydroxylapatite, HydAp), and organic phosphate (phytic acid, PhyAc).³⁸ S reference compounds include FeS, pyrite (FeS_2),³⁹ cysteine,⁴⁰ cystine, methionine methylsulfonium chloride, methionine sulfoxide, methionine sulfone, anthraquinone sulfonic acid,⁴¹ chondroitine sulfate,⁴² and CaSO_4 . Details on these reference compounds are described in Table S2.

2.4. Sequential Chemical Extraction. To evaluate the mobility and phase distribution of P, sequential chemical extraction was performed on the dry and ground sludge mixture, hydrochars, and AD solids following Hedley's method.⁴³ Briefly, 0.15 g of each sample was sequentially extracted in deionized (DI) water, 0.5 mol/L NaHCO_3 , 0.1 mol/L NaOH , and 1.0 mol/L HCl . Solid sample was shaken in a 50 mL polypropylene centrifuge tube with 20 mL of each extraction solution for 16 h at 20 °C. The residue after the 1.0 mol/L HCl extraction was digested by aqua regia. The reacted suspension from each extraction step was centrifuged, and an aliquot of the supernatant was vacuum filtered (0.45 μm) and analyzed for total P concentration using the molybdate–

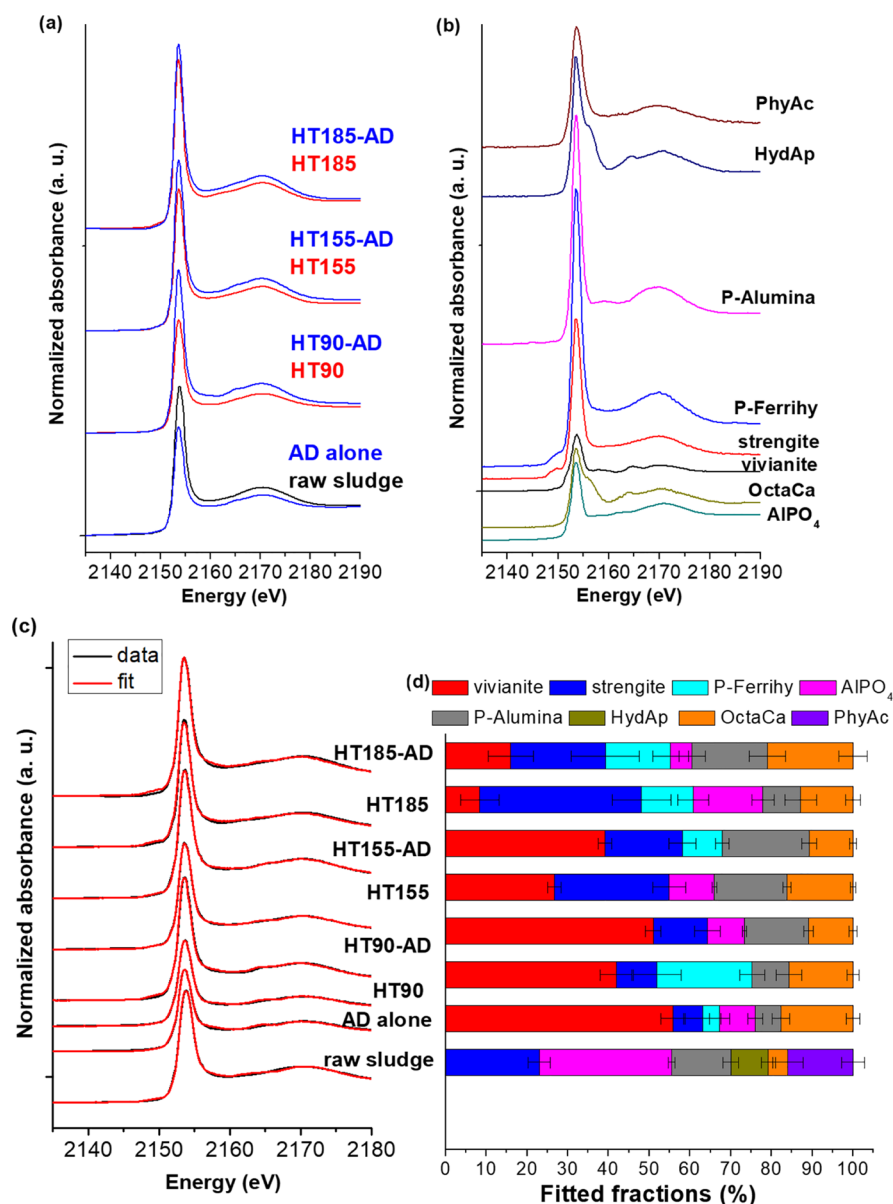


Figure 2. P K-edge XANES results. (a) XANES spectra of raw sludge, AD-alone solid, HT hydrochars, and AD solids after HT treatment at 90, 155, or 185 °C. (b) XANES spectra of reference compounds used for linear combination fitting (LCF) analyses, including AlPO₄, octacalcium phosphate (OctaCa), vivianite, strengite, phosphate sorbed on ferrihydrite (P-Ferrihy), phosphate sorbed on γ -alumina (P-Alumina), hydroxylapatite (HydAp), and phytic acid (PhyAc). (c) Raw and fitted spectra. (d) Relative percentage of contributing P species determined by LCF.

ascorbic acid method with an UV–vis spectrophotometer (Carey 60, Agilent).⁴⁴ Each sample was subjected to the same sequential extraction procedure for two times, and P concentration was determined for two times per sample.

3. RESULTS AND DISCUSSION

3.1. Elemental Composition of Treated Solids. Both HT and AD strongly affected the elemental concentrations in the solids. Table S3 presents the total concentrations of Fe, P, and S in the raw sludge mixture, HT hydrochars, AD solids, HT process water, and AD process water. Fe concentration in the HT process water and AD process water was below 30 μ M, consistent with literature results where heavy metals mostly remain in the solids after HT or AD.^{14,20} Fe concentration in the HT hydrochars increased with HT temperature. For instance, Fe concentrations of the raw sludge mixture and

HT185 hydrochar were 0.93% and 4.89%, respectively (Table S3). Except for sample HT185-AD, AD increased the Fe concentration in the AD solids due to conversion of organic matter to biogas and the addition of anaerobic inoculum (which contains 3.15% Fe). Fe concentration in HT185-AD solid decreased as a result of mixing with the anaerobic inoculum.

Similar trends were observed for P in the HT hydrochars and AD solids (Table S3). However, compared with the supernatant of raw sludge, the P concentration in the HT process water increased with no significant difference under different HT temperatures (Table S3). During the subsequent AD process, P concentration in the AD process water increased significantly, suggesting that a portion of P was released during AD. The S concentration was similar in the HT90 and HT155 hydrochars, whereas it decreased significantly in the HT185

hydrochar (Table S3). This was probably due to the cracking of the unstable mercaptan structure of organic S to produce sulfides.⁴⁵ Thus, the process water derived from higher HT temperatures had higher S concentrations (Table S3) due to the release of S from the decomposition of organic S.³⁰ Meanwhile, compared with raw sludge and HT-alone samples, S concentration in the AD solids increased significantly while it decreased in the AD process waters, suggesting that more S remained in the solids after AD. A previous study reported that H₂S appeared in biogas during AD, but more sulfate and organic S preferentially remained in solid and solution phases at a higher initial pH of 8.²⁵ This is consistent with our work where little H₂S gas was detected by gas chromatography (data not shown) and the initial pH for the AD matrix was 7.7–8.0.

3.2. Fe Speciation in the Solids. XAS is useful in direct determination of Fe speciation. The XANES region is sensitive to changes in the oxidation state (Figure S3). Compared with Fe XANES spectra of the raw sludge mixture, the position of the main edge and pre-edge peak of the HT hydrochars shifted to lower energy, suggesting the reduction of Fe(III) to Fe(II). However, such energy shifting became less significant with increasing HT temperature, suggesting that HT at higher temperature inhibited Fe(III) reduction, resulting in less Fe(II) in the HT hydrochars. Significant Fe(III) reduction was observed for AD-alone sample (Figure S3). Similar but less significant changes were also observed for the AD solids. For the HT90 and HT185 hydrochars, AD did not cause much further Fe(III) reduction.

Figure 1a shows the *k*³-weighted Fe EXAFS spectra for the solids. The raw sludge mixture had characteristic oscillations at 4.2, 6.5, 8.5, and 10.0 Å⁻¹. For HT90 hydrochar, the oscillations at 4.2 and 6.5 Å⁻¹ shifted to lower energies and the other two oscillations became flattened. Meanwhile, two oscillations at 5.1 and 7.5 Å⁻¹ appeared (Figure 1a and 1b), which are diagnostic features for vivianite.^{34,46} However, these two peaks were much weaker for HT155 and HT185 hydrochars, indicating less or no vivianite formation at 155 and 185 °C. Changes similar to sample HT90 were also observed for the AD-alone sample. This suggests that direct AD of raw sludge produced significant amounts of vivianite, consistent with previous studies.^{3,20} Compared to sample HT90, the changes in the spectra of sample HT90-AD were very subtle. The oscillations at 5.1 and 7.5 Å⁻¹ became slightly more pronounced for samples HT155-AD and HT185-AD than those of samples HT155 and HT185.

To quantify Fe speciation in the solids, LCF analysis was conducted on Fe K-edge EXAFS spectra using a library of relevant Fe reference compounds. Best-fitting results (i.e., with the lowest *R* factor values) were obtained using vivianite, strengite, ferrihydrite, and Fe(III)–organic complex. Addition of either carbonated green rust or siderite was required but yielded similar *R* factors (Tables S4 and S5, Figures 1 and S4). Strengite, ferrihydrite, and Fe(III)–organic complex are Fe(III) species, vivianite and siderite are Fe(II) species, and green rust contains both Fe(II) and Fe(III). For HT90 hydrochar, the fraction of Fe(III) species decreased while vivianite formed at up to 60.4%. This is due to the reductive dissolution of Fe(III), release of dissolved Fe(II), and subsequent precipitation of vivianite in the presence of soluble phosphate. With increasing HT temperature (155 and 185 °C), the fractions of Fe(III)–organic complex and ferrihydrite decreased while the fraction of strengite increased. Meanwhile, formation of vivianite was minimal. This suggests that a higher

HT temperature prohibited Fe(III) reduction, and the released Fe(III) from decomposition of Fe(III)–organic complex precipitated with phosphate to form strengite. Similar results as HT90 sample were observed for AD-alone sample. For the hydrochars, the subsequent AD led to further Fe(III) reduction and formation of more vivianite (Tables S4 and S5, Figures 1 and S4).

Both carbonated green rust and siderite can be present in sludges.^{22,47,48} Inclusion of either one as a reference compound yielded similar goodness of fitting and similar trends for the other four dominant Fe species (vivianite, strengite, Fe(III)–organic complex, and ferrihydrite) (Tables S4 and S5, Figures 1 and S4). The differences are that the fraction of carbonated green rust (~20%) did not change much (Table S4 and Figure S4) while the fraction of siderite (23.5%) decreased significantly after HT–AD processes (Table S5 and Figure 1). Note that the fractionation values obtained by LCF have an error of <10%. The uncertainty in fitting in terms of both the identity and the quantity of possible end members also accounts for the intrinsic insensitivity of LCF in distinguishing species with similar spectral features. However, exchange of carbonated green rust with siderite does not affect the overall trends in the evolution of Fe speciation.

3.3. P Speciation in the Solids. Figures 2a and S5 show the P K-edge XANES spectra of the solids. The spectrum of vivianite has a characteristic oscillation at 2161 to 2166 eV,³⁷ which is observed for all AD solids except for sample HT185-AD (Figure S5). This is consistent with the Fe EXAFS observed presence of vivianite in these samples as shown in Figure 1.

LCF analysis was also conducted on P XANES to determine the contributing P species and their relative abundance in the solids. Reference compounds listed in Table S2 yielded the best-fitting results (Figure 2c and 2d and Table S6). Strengite (23.0%), AlPO₄ (32.5%), alumina-adsorbed phosphate (14.5%), hydroxylapatite (9.2%), and phytic acid (16.0%) were the main species identified in the raw sludge mixture. Inorganic P species dominated in the hydrochars and AD solids due to the decomposition and hydrolysis of organic P.^{2,10,49} Compared with the raw sludge, vivianite, ferrihydrite-adsorbed phosphate, and octacalcium phosphate in HT90 hydrochar increased to 41.9%, 23.3%, and 15.7%, respectively, while the relative abundances of strengite, AlPO₄, and hydroxylapatite decreased. With increasing HT temperature, the abundance of vivianite in HT155 and HT185 hydrochars decreased, while the relative abundance of strengite and AlPO₄ increased. For example, the contents of vivianite, strengite, and AlPO₄ in HT185 hydrochars were 8.4%, 39.7%, and 17.1%, respectively (Figure 2d and Table S6). In the subsequent AD solids, vivianite content increased while strengite and AlPO₄ contents decreased. In addition, the contents of ferrihydrite-adsorbed phosphate and alumina-adsorbed phosphate increased slightly in HT155-AD and HT185-AD hydrochars. For HT185-AD, the contents of vivianite, strengite, and AlPO₄ in HT185 were 16.0%, 23.2%, and 5.3%, respectively (Figure 2d and Table S6).

Sequential chemical extraction was used to provide further information on P speciation and mobility. Figure 3 shows the relative abundance of each P species in the solid samples by sequential extraction. For the raw sludge mixture, ~35% of P was present in the soluble (water extractable) and adsorbed fractions (NaHCO₃ extractable). About 50% of P was associated with Al/Fe minerals (NaOH extractable). Insoluble

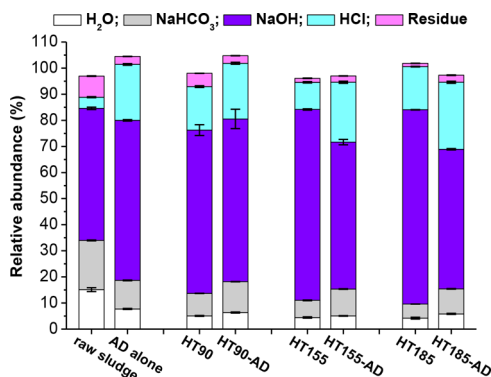


Figure 3. P speciation determined by sequential chemical extraction of the raw sludge, AD-alone solid, HT hydrochars, and AD solids after HT at 90, 155, or 185 °C. Error bars indicate the standard deviation of measurements ($n = 4$).

P species (HCl extractable) accounted for approximately 3% of total P. Note that the P content in these sequential extracts was analyzed as inorganic P (details in the experimental section). By calculating the difference between total P and the P concentration in the extracts, the fraction of organic P was

negligible after the HT-AD (Figure 3), suggesting an almost complete conversion of organic P to inorganic P after HT-AD. For the hydrochars, P components in the solids became less soluble and exchangeable with increasing HT temperature. For instance, about 10% of P remained as soluble and adsorbed fractions in HT185 hydrochar, while the fractions of P associated with Al/Fe and insoluble P reached up to ~75% and ~15%, respectively (Figure 3). After AD, soluble, desorbed, and insoluble fractions of P in the AD solids increased while the fraction of P associated with Al/Fe decreased. For HT185-AD, the soluble and adsorbed fractions and the insoluble fraction of P were ~16.5% and ~26%, respectively, while P associated with Al/Fe fraction was 51%.

3.4. S Speciation in the Solids. S K-edge XANES spectroscopy is sensitive for distinguishing different oxidation states of S in solids.⁴⁰ Figure 4a presents the S K-edge XANES spectra of the solid samples. The oscillations at 2472.6, 2473.2, 2481.0, and 2482.5 eV are characteristic for zerovalent S, thiols ($S^{+0.5}$), sulfonates (S^{+5}), and sulfates (S^{+6}) (Figure 4b), respectively.⁴⁰ Compared to the raw sludge mixture, the peak intensities of S^{+5} and S^{+6} for hydrochars decreased slightly with increasing HT temperature as well as for the AD solids, suggesting a decrease in the contents of these species. The

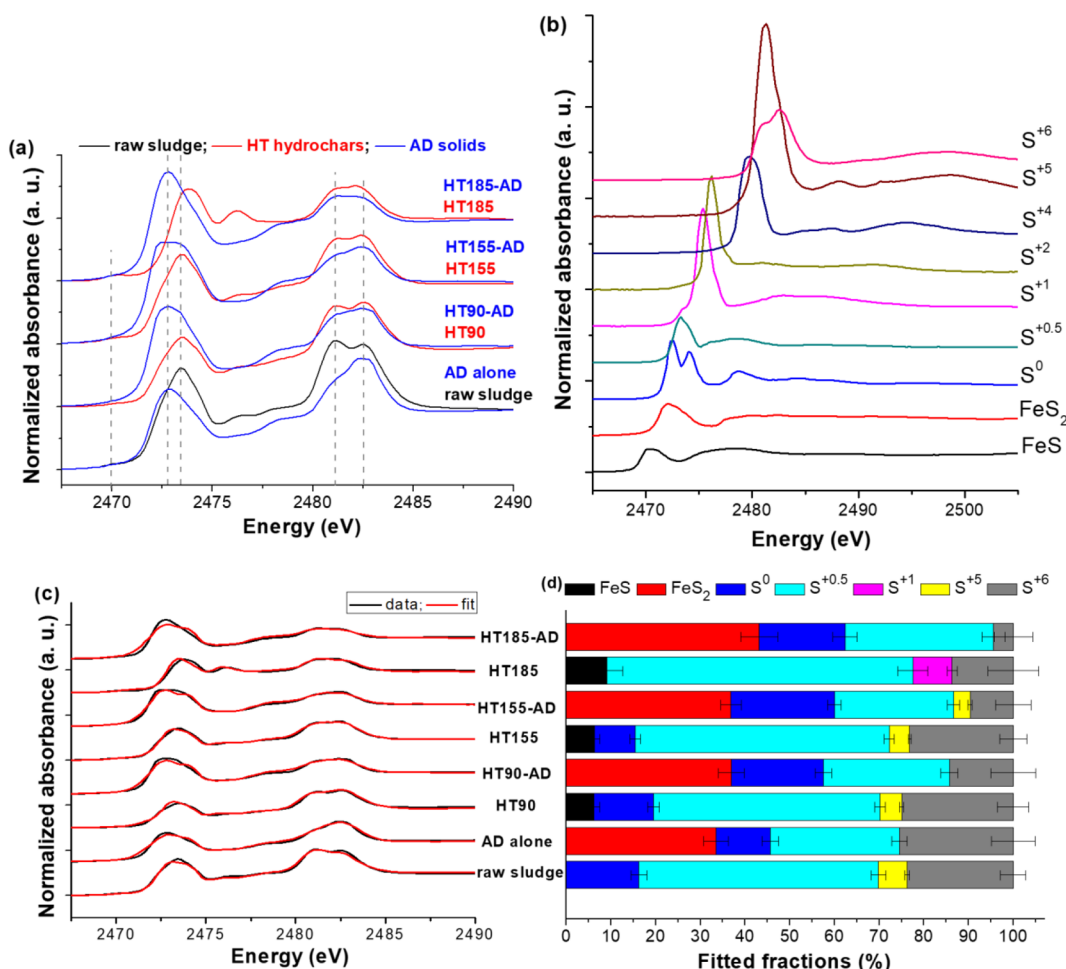


Figure 4. S K-edge XANES results. (a) XANES spectra of raw sludge, AD-alone solid, HT hydrochars, and AD solids after HT treatment at 90, 155, or 185 °C. (b) XANES spectra of reference compounds used for linear combination fitting (LCF) analyses, including FeS, FeS₂, cystine (S^0), cysteine ($S^{+0.5}$), sulfonium (S^{+1}), sulfoxide (S^{+2}), sulfone (S^{+4}), sulfonate (S^{+5}), and sulfate (S^{+6}). (c) Raw and fitted spectra. (d) Relative percentage of contributing S species determined by LC.

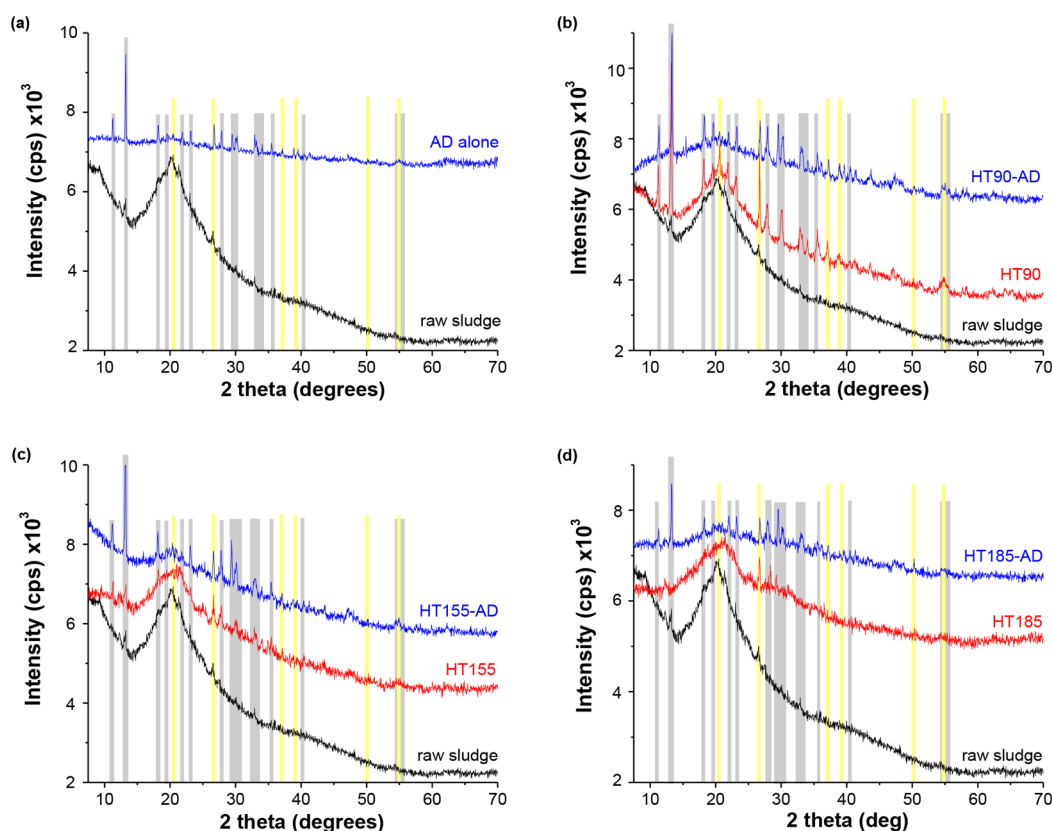


Figure 5. XRD patterns of the raw sludge, AD-alone solid, HT hydrochars, and AD solids after HT at 90, 155, or 185 °C. Gray and yellow vertical bars indicate XRD peak positions for vivianite (PDF no. 83-2453) and quartz (PDF no. 46-1045), respectively.

position of the peak at 2473.2 eV was almost the same for HT90 and HT155 samples but shifted to 2474 eV for HT185 accompanied by the appearance of a new peak at 2476 eV, suggesting a change in the major S species, as discussed below in LCF analysis. For the subsequent AD final solids, the peaks at 2473.2 and 2474 eV shifted to lower energy and the peak at 2476 eV disappeared due to the extensive S reduction during AD processes.

Prietz et al.⁴⁰ analyzed S speciation in soils by comparing LCF and Gaussian curve fitting (GCF) of S K-edge XANES data and recommended using LCF when appropriate reference compounds are available. In this study, LCF analysis was conducted on S XANES spectra of the solid samples using a range of S reference compounds (Figure 4c and 4d, Table S7). The major chemical forms of S in the solids existed in the oxidation states similar to FeS, pyrite, S⁰, thiols (S^{+0.5}), sulfonates (S⁺⁵), and sulfates (S⁺⁶). Note that LCF using these S reference compounds is more sensitive for probing the oxidation state instead of the exact compound structure.^{23,40,50} For the raw sludge mixture, the main S species were zerovalent S (~15%), thiols (S^{+0.5}, ~52%), sulfonates (S⁺⁵, ~6%), and sulfates (S⁺⁶, ~20%). For the HT hydrochars, the fractions of zerovalent S, sulfonates, and sulfates decreased with increasing HT temperature. For HT185 sample, the fraction of sulfates decreased to 12% and zerovalent S and sulfonates disappeared. S⁺¹ species appeared in the HT185 sample, accounting for the occurrence of the new peak at 2476 eV. In addition, a new phase FeS appeared, and its fraction increased to 8.0%. For the subsequent AD final solids, the dominant S species were pyrite, S⁰, S^{+0.5}, and S⁺⁶. The fractions of S^{+0.5} and S⁺⁶ decreased, while the fractions of pyrite and S⁰ increased with pyrite

accounting for 33–40% of total S. Considering that the error of S K-edge LCF analyses is typically ~10%,⁴⁰ note that our fitting results mainly reflected the changing trends of the inorganic and organic S species with different states during HT–AD processes.

3.5. Mineral Phase Evolution. XRD analysis confirmed the changes in mineralogy as revealed by XAS analyses. Figure 5 shows the XRD patterns of the raw sludge mixture, hydrochars, and AD solids. The raw sludge mixture has a few weak diffraction peaks associated with minor amounts of quartz and other crystalline phases that were difficult to accurately identify. The presence of vivianite in HT90 hydrochar was confirmed by XRD. Weak peaks of vivianite were observed for HT155 hydrochar, whereas these peaks were absent in HT185 hydrochar. For the AD final solids, the peaks of vivianite became stronger, suggesting formation of more vivianite. These observations are consistent with Fe EXAFS and P XANES LCF analyses. In addition, the peaks of quartz became stronger after HT/AD treatments (Figure 5), as conversion of organic matter into biogas enhanced the quartz concentration in hydrochars and AD solids.

Precipitation of struvite (MgNH₄PO₄·6H₂O) was previously observed in anaerobically digested sludge or manure.^{51,52} In this study, however, no struvite in AD solids was detected by XRD (Figure 5). In addition, XPS spectra of selected AD solid samples showed that the total N content in these solids was low (Figure S6). Prior studies reported that the presence of metal ions (e.g., Ca²⁺, Fe³⁺, Cu²⁺, or Zn²⁺) can inhibit struvite crystallization.^{52–55} For instance, addition of FeCl₃ was used to prevent struvite precipitations in anaerobic digesters.⁵⁶ In our study, the concentrations of Fe, Ca, and Al in the raw sludge

mixture were much higher than that of Mg (Table S1). Therefore, Fe, Ca, and Al might have preferentially reacted with P rather than formation of struvite in AD processes.

3.6. Coupled Cycling of Fe and P. During HT–AD, the speciation of Fe significantly correlated with that of P. The reduction of Fe(III) to Fe(II) was strongly mediated by phosphate availability and formation of Fe–P minerals, which in turn also affected P mineralogy and mobility/bioavailability, as detailed below.

The reduction of Fe(III) during HT was likely coupled with the oxidation of organic matter. Cellulose (a major component of organic matter in municipal sludge) cannot directly reduce Fe(III), but its breakdown products can reduce Fe(III).¹⁵ HT of sewage sludge mainly consists of a series of reactions, including hydrolysis, dehydration, decarboxylation, aromatization, and condensation.⁵⁷ During HT, hydrolysis of cellulose produces glucose, which is further hydrolyzed to produce furfural derivatives such as 5-hydroxymethylfurfural (5-HMF). These intermediates (i.e., 5-HMF) can reduce Fe(III) to Fe(II) under hydrothermal conditions.^{17,58} During HT of sewage sludge, reduction of FeOOH in the absence of oxyanions forms magnetite,^{15,17} whereas oxyanions (e.g., phosphate and carbonate) can complex with the produced Fe(II) and form secondary mineral precipitates such as vivianite and siderite.⁵⁹ The presence of phosphate inhibits formation of magnetite and green rust⁶⁰ but can lead to preferential formation of the stable phase vivianite.⁶¹ Our LCF analysis of Fe EXAFS data did not detect the presence of magnetite, which is likely due to the inhibition effect from the presence of a high concentration of phosphate. However, the presence of carbonated green rusts or siderite (~20%) was observed from LCF analyses, which was introduced from raw sludge. Compared with raw sludge, the fraction of carbonated green rust did not change much while it decreased for siderite during HT–AD processes.

During high-temperature HT, intermediates such as glucose, fructose, and 5-HMF can further lead to formation of polyfuranic-type compounds through polymerization–polycondensation and finally produce hydrochars with a polyaromatic hydrocarbon network by aromatization.⁶² However, Fe(III) cannot be easily reduced by hydrochar. Thus, compared with the HT90 sample, less formation of vivianite occurred in HT155 and HT185 samples due to less Fe(III) reduction. During HT treatments at 155 and 185 °C, decomposition of Fe(III)–OM released Fe(III), which precipitated with phosphate to form strengite. Besides the soluble inorganic phosphate originally present in the raw sludge mixture, the other source of soluble inorganic phosphate was from organic P decomposition during the HT process.²

During the subsequent AD process, a variety of microorganisms are responsible for dissimilatory Fe(III) reduction coupled with organic matter oxidation.^{63,64} This biotic reaction provides a major source of Fe(II), which precipitated with soluble phosphate to form vivianite. The soluble phosphate could be the result of reductive dissolution of strengite⁶⁵ and/or degradation of organic P.⁶⁶

As enhanced biological phosphorus removal (EBPR) is employed in the WRRF where samples were obtained in this study, the Fe/P molar ratio in the raw sludge was not relatively low (i.e., 0.27 in this study). It was much lower than those plants relying on chemical phosphorus removal by Fe dosing. The main Fe speciation may be different, but the precipitation

of vivianite in the anaerobically digested sludge might still dominate for P speciation. This finding was confirmed by several previous studies.^{3,20,21}

3.7. Coupled Cycling of Fe and S. The contents of Fe sulfides were very low in both hydrochars and AD solids, but precipitation of Fe sulfides may shed light on the coupled cycling of Fe and S during HT and AD processes. During the hydrothermal process, hydrolysis of organic S with high oxidation state produces reduced S species such as sulfide,^{12,14} which can subsequently precipitate with dissolved metal ions (e.g., Fe²⁺, Cu²⁺, Zn²⁺) and form metal sulfides.^{12,14,67}

The AD process favors formation of sulfides as the dominant S species.²⁴ During AD, microbial reduction of sulfate and organic S produces a large amount of hydrogen sulfide.^{68–70} Fe(III) can be also reduced by sulfides to form Fe sulfides.⁶⁴ We did not observe FeS formation but instead observed pyrite accumulation in the AD solids, possibly due to the reaction of FeS with excessive hydrogen sulfide.^{71–73} Although formation of pyrite is considered to be a slow process under anaerobic condition, several previous studies have reported the presence of pyrite in anaerobically digested sludge.^{20,29} This is consistent with natural processes (such as those occurring in sediments) on the transformation of FeS to pyrite.^{71–73} The fraction of pyrite in the AD solids was up to 42% of total S based on LCF of S XANES data (Figure 4d and Table S7). Considering that S LCF analyses mainly serve as a tool for understanding S oxidation states, we note that the 42% fitted pyrite may include other metal sulfides^{74,75} because the concentrations of other heavy metals (e.g., Cu and Zn) in the raw sludge are also high (Table S1).

4. ENVIRONMENTAL IMPLICATIONS

Sewage sludge typically contains large amounts of organic matter, nutrients, and heavy metals.^{24,76,77} Sequential HT–AD is a potential sustainable technology for the recovery of resources from sludge. To better select HT operation conditions, it is critical to understand how HT temperature affects the transformations of major redox elements (e.g., Fe and S) and nutrient elements (e.g., P) during the overall HT–AD processes.

Our results indicate that HT pretreatment at low temperature (90 °C) favored the production of vivianite, while strengite was preferably produced at higher temperatures (155 and 185 °C). HT pretreatment at high temperatures inhibited the extent of vivianite production during the subsequent AD process. Our findings provide fundamental insights on the fate of Fe and P in sewage sludge during the HT–AD process, which has implications in vivianite recovery from sludge.^{28,78–80} Because the speciation of Fe was largely coupled with the P cycles, the speciation information on both Fe and P is critical to evaluate P recycling/reclamation and selection and optimization treatment solutions. Formation of vivianite also favors immobilization of arsenic in sludges, because arsenate can be coprecipitated with vivianite.^{81,82} In addition, S affected the mobility and availability of Fe. A small amount of ferrous sulfide was formed by HT treatments, while a high content of pyrite was found in the subsequent AD process. Our results also provide important information on S speciation (i.e., oxidation state) in the hydrochars and AD solids, which is of agricultural and environmental interest.⁸³ For instance, information on S speciation can help understand S bioavailability during the land application of AD solids.^{83,84} Iron sulfides can contain a certain amount of metals (i.e., Pb,

Cd, Cu) via adsorption and/or coprecipitation, affecting the solubility and bioavailability of the toxic metals.⁸⁵ In addition, some toxic metals such as Cd and Hg can precipitate with sulfides in the treated sludges. Considering the presence of Cu and Zn (Table S1), future studies are warranted on the impact of HT pretreatment on the evolution of Cu- and Zn-sulfides in AD solids.

■ ASSOCIATED CONTENT

Supporting Information

The Supporting Information is available free of charge at <https://pubs.acs.org/doi/10.1021/acs.est.0c00501>.

Text for XAS, XRD, and XPS analyses; tables for the treatment conditions and sample labels, reference compounds used for XAS LCF analyses, and results of the major elemental concentrations in the solids and process waters; figures of Fe and P K-edge XANES analysis, Fe, P, and S LCF results, and XPS data (PDF)

■ AUTHOR INFORMATION

Corresponding Author

Yuanzhi Tang – School of Earth and Atmospheric Sciences and School of Civil and Environmental Engineering, Georgia Institute of Technology, Atlanta, Georgia 30332-0340, United States; orcid.org/0000-0002-7741-8646; Phone: 404-894-3814; Email: yuanzhi.tang@eas.gatech.edu

Authors

Qian Wang – School of Earth and Atmospheric Sciences, Georgia Institute of Technology, Atlanta, Georgia 30332-0340, United States

Chiqian Zhang – School of Civil and Environmental Engineering, Georgia Institute of Technology, Atlanta, Georgia 30332-0512, United States; orcid.org/0000-0003-4532-7376

Dhara Patel – School of Earth and Atmospheric Sciences, Georgia Institute of Technology, Atlanta, Georgia 30332-0340, United States

Haesung Jung – School of Earth and Atmospheric Sciences, Georgia Institute of Technology, Atlanta, Georgia 30332-0340, United States

Pan Liu – School of Earth and Atmospheric Sciences, Georgia Institute of Technology, Atlanta, Georgia 30332-0340, United States

Biao Wan – School of Earth and Atmospheric Sciences, Georgia Institute of Technology, Atlanta, Georgia 30332-0340, United States

Spyros G. Pavlostathis – School of Civil and Environmental Engineering, Georgia Institute of Technology, Atlanta, Georgia 30332-0512, United States; orcid.org/0000-0001-9731-3836

Complete contact information is available at: <https://pubs.acs.org/doi/10.1021/acs.est.0c00501>

Notes

The authors declare no competing financial interest.

■ ACKNOWLEDGMENTS

This work utilizes the EXAFS spectra of Fe reference compounds kindly provided by Dr. Atsushi Ikeda-Ohno and Dr. T. David Waite, Dr. Chunmei Chen, or Dr. Colleen M. Hansel. We thank Dr. Matthias Egger, Dr. Rixiang Huang, and

Dr. Florian Werner for sharing their XANES spectra of P reference compounds. We appreciate Dr. Magnus Sandström, Dr. Sylvain Bohic, Dr. Jörg Prietzel, Dr. Jean-Pierre Cuif, and Dr. Andréas Scheinost for sharing their XANES spectra of S reference compounds. The detailed information can be found in the SI Table S2. We acknowledge beamline scientists at BL 4-1 and BL 14-3 at the Stanford Synchrotron Radiation Lightsource (SSRL) for technical assistance on data collection. A portion of his research was conducted at SSRL, a U.S. Department of Energy (DOE) Office of Science User Facility operated for the DOE Office of Science by SLAC National Accelerator Laboratory under Contract No. DE-AC02-76SF00515.

■ REFERENCES

- (1) Wei, Y.; Van Houten, R. T.; Borger, A. R.; Eikelboom, D. H.; Fan, Y. Minimization of excess sludge production for biological wastewater treatment. *Water Res.* **2003**, *37* (18), 4453–4467.
- (2) Huang, R.; Tang, Y. Speciation dynamics of phosphorus during (hydro)thermal treatments of sewage sludge. *Environ. Sci. Technol.* **2015**, *49* (24), 14466–14474.
- (3) Wilfert, P.; Dugulan, A. I.; Goubitz, K.; Korving, L.; Witkamp, G. J.; Van Loosdrecht, M. C. M. Vivianite as the main phosphate mineral in digested sewage sludge and its role for phosphate recovery. *Water Res.* **2018**, *144*, 312–321.
- (4) Li, C.; Wang, X.; Zhang, G.; Li, J.; Li, Z.; Yu, G.; Wang, Y. A process combining hydrothermal pretreatment, anaerobic digestion and pyrolysis for sewage sludge dewatering and co-production of biogas and biochar: Pilot-scale verification. *Bioresour. Technol.* **2018**, *254*, 187–193.
- (5) Pilli, S.; Yan, S.; Tyagi, R. D.; Surampalli, R. Y. Thermal pretreatment of sewage sludge to enhance anaerobic digestion: a review. *Crit. Rev. Environ. Sci. Technol.* **2015**, *45* (6), 669–702.
- (6) Li, C.; Wang, X.; Zhang, G.; Yu, G.; Lin, J.; Wang, Y. Hydrothermal and alkaline hydrothermal pretreatments plus anaerobic digestion of sewage sludge for dewatering and biogas production: Bench-scale research and pilot-scale verification. *Water Res.* **2017**, *117*, 49–57.
- (7) Passos, F.; Ferrer, I. Influence of hydrothermal pretreatment on microalgal biomass anaerobic digestion and bioenergy production. *Water Res.* **2015**, *68*, 364–373.
- (8) Akiya, N.; Savage, P. E. Roles of water for chemical reactions in high-temperature water. *Chem. Rev.* **2002**, *102* (8), 2725–2750.
- (9) Shi, Y.; Luo, G.; Rao, Y.; Chen, H.; Zhang, S. Hydrothermal conversion of dewatered sewage sludge: Focusing on the transformation mechanism and recovery of phosphorus. *Chemosphere* **2019**, *228*, 619–628.
- (10) Huang, R.; Tang, Y. Evolution of phosphorus complexation and mineralogy during (hydro)thermal treatments of activated and anaerobically digested sludge: Insights from sequential extraction and P K-edge XANES. *Water Res.* **2016**, *100*, 439–447.
- (11) Wang, T.; Zhai, Y.; Zhu, Y.; Peng, C.; Wang, T.; Xu, B.; Li, C.; Zeng, G. Feedwater pH affects phosphorus transformation during hydrothermal carbonization of sewage sludge. *Bioresour. Technol.* **2017**, *245*, 182–187.
- (12) Liang, Y.-J.; Chai, L.-Y.; Min, X.-B.; Tang, C.-J.; Zhang, H.-J.; Ke, Y.; Xie, X.-D. Hydrothermal sulfidation and floatation treatment of heavy-metal-containing sludge for recovery and stabilization. *J. Hazard. Mater.* **2012**, *217–218*, 307–314.
- (13) Min, X.; Yuan, C.; Liang, Y.; Chai, L.; Ke, Y. Metal recovery from sludge through the combination of hydrothermal sulfidation and floatation. *Procedia Environ. Sci.* **2012**, *16*, 401–408.
- (14) Huang, R.; Zhang, B.; Saad, E. M.; Ingall, E. D.; Tang, Y. Speciation evolution of zinc and copper during pyrolysis and hydrothermal carbonization treatments of sewage sludges. *Water Res.* **2018**, *132*, 260–269.

- (15) Hage, J. L. T.; Schuiling, R. D.; Vriend, S. P. Production of magnetite from sodiumjarosite under reducing hydrothermal conditions. The reduction of Fe^{III} to Fe^{II} with cellulose. *Can. Metall. Q.* **1999**, *38* (4), 267–276.
- (16) Zhang, H.; Xue, G.; Chen, H.; Li, X. Magnetic biochar catalyst derived from biological sludge and ferric sludge using hydrothermal carbonization: Preparation, characterization and its circulation in Fenton process for dyeing wastewater treatment. *Chemosphere* **2018**, *191*, 64–71.
- (17) Gu, L.; Li, B.; Wen, H.; Zhang, X.; Wang, L.; Ye, J. Co-hydrothermal treatment of fallen leaves with iron sludge to prepare magnetic iron product and solid fuel. *Bioresour. Technol.* **2018**, *257*, 229–237.
- (18) Sommers, L. E. Chemical composition of sewage sludges and analysis of their potential use as fertilizers. *J. Environ. Qual.* **1977**, *6* (2), 225–232.
- (19) Stabnikov, V. P.; Tay, S. T.-L.; Tay, D.-K.; Ivanov, V. N. Effect of iron hydroxide on phosphate removal during anaerobic digestion of activated sludge. *Appl. Biochem. Microbiol.* **2004**, *40* (4), 376–380.
- (20) Wilfert, P.; Mandalidis, A.; Dugulan, A. I.; Goubitz, K.; Korving, L.; Temmink, H.; Witkamp, G. J.; Van Loosdrecht, M. C. M. Vivianite as an important iron phosphate precipitate in sewage treatment plants. *Water Res.* **2016**, *104*, 449–460.
- (21) Wu, Y.; Luo, J.; Zhang, Q.; Aleem, M.; Fang, F.; Xue, Z.; Cao, J. Potentials and challenges of phosphorus recovery as vivianite from wastewater: A review. *Chemosphere* **2019**, *226*, 246–258.
- (22) Prot, T.; Nguyen, V. H.; Wilfert, P.; Dugulan, A. I.; Goubitz, K.; De Ridder, D. J.; Korving, L.; Rem, P.; Bouderbala, A.; Witkamp, G. J.; van Loosdrecht, M. C. M. Magnetic separation and characterization of vivianite from digested sewage sludge. *Sep. Purif. Technol.* **2019**, *224*, 564–579.
- (23) Van Hullebusch, E.; Rossano, S.; Farges, F.; Lenz, M.; Labanowski, J.; Lagarde, P.; Flank, A.; Lens, P. In Sulfur K-edge XANES spectroscopy as a tool for understanding sulfur chemical state in anaerobic granular sludge. *J. Phys.: Conf. Ser.* **2009**, *190*, 012184.
- (24) Dewil, R.; Baeyens, J.; Roels, J.; Van De Steene, B. Distribution of sulphur compounds in sewage sludge treatment. *Environ. Eng. Sci.* **2008**, *25* (6), 879–886.
- (25) Yan, L.; Ye, J.; Zhang, P.; Xu, D.; Wu, Y.; Liu, J.; Zhang, H.; Fang, W.; Wang, B.; Zeng, G. Hydrogen sulfide formation control and microbial competition in batch anaerobic digestion of slaughterhouse wastewater sludge: Effect of initial sludge pH. *Bioresour. Technol.* **2018**, *259*, 67–74.
- (26) Lippens, C.; De Vrieze, J. Exploiting the unwanted: Sulphate reduction enables phosphate recovery from energy-rich sludge during anaerobic digestion. *Water Res.* **2019**, *163*, 114859.
- (27) Fang, C.; Huang, R.; Dykstra, C.; Jiang, R.; Pavlostathis, S. G.; Tang, Y. Energy and nutrient recovery from sewage sludge and manure via anaerobic digestion with hydrothermal pretreatment. *Environ. Sci. Technol.* **2020**, *54* (2), 1147–1156.
- (28) Wilfert, P.; Kumar, P. S.; Korving, L.; Witkamp, G.-J.; van Loosdrecht, M. C. M. The relevance of phosphorus and iron chemistry to the recovery of phosphorus from wastewater: A review. *Environ. Sci. Technol.* **2015**, *49* (16), 9400–9414.
- (29) Kaksonen, A. H.; Riekkola-Vanhanen, M. L.; Puhakka, J. A. Optimization of metal sulphide precipitation in fluidized-bed treatment of acidic wastewater. *Water Res.* **2003**, *37* (2), 255–266.
- (30) Appels, L.; Degrève, J.; Van der Bruggen, B.; Van Impe, J.; Dewil, R. Influence of low temperature thermal pre-treatment on sludge solubilisation, heavy metal release and anaerobic digestion. *Bioresour. Technol.* **2010**, *101* (15), 5743–5748.
- (31) Wilson, C. A.; Novak, J. T. Hydrolysis of macromolecular components of primary and secondary wastewater sludge by thermal hydrolytic pretreatment. *Water Res.* **2009**, *43* (18), 4489–4498.
- (32) Ravel, B.; Newville, M. ATHENA, ARTEMIS, HEPHAESTUS: data analysis for X-ray absorption spectroscopy using IFEFFIT. *J. Synchrotron Radiat.* **2005**, *12* (4), 537–541.
- (33) Hansel, C. M.; Benner, S. G.; Neiss, J.; Dohnalkova, A.; Kukkadapu, R. K.; Fendorf, S. Secondary mineralization pathways induced by dissimilatory iron reduction of ferrihydrite under advective flow. *Geochim. Cosmochim. Acta* **2003**, *67* (16), 2977–2992.
- (34) Wu, H.; Ikeda-Ohno, A.; Wang, Y.; Waite, T. D. Iron and phosphorus speciation in Fe-conditioned membrane bioreactor activated sludge. *Water Res.* **2015**, *76*, 213–226.
- (35) Wu, H.; Wang, Y.; Ikeda-Ohno, A.; Miller, C. J.; Waite, T. D. Impact of ferrous iron dosing on iron and phosphorus solids reduction and transformation in a pilot scale membrane bioreactor. *Environ. Sci.: Water Res. Technol.* **2019**, *5* (8), 1400–1411.
- (36) Chen, C.; Dynes, J. J.; Wang, J.; Sparks, D. L. Properties of Fe-organic matter associations via coprecipitation versus adsorption. *Environ. Sci. Technol.* **2014**, *48* (23), 13751–13759.
- (37) Egger, M.; Jilbert, T.; Behrends, T.; Rivard, C.; Slomp, C. P. Vivianite is a major sink for phosphorus in methanogenic coastal surface sediments. *Geochim. Cosmochim. Acta* **2015**, *169*, 217–235.
- (38) Werner, F.; Prietzel, J. Standard protocol and quality assessment of soil phosphorus speciation by P K-edge XANES spectroscopy. *Environ. Sci. Technol.* **2015**, *49* (17), 10521–10528.
- (39) Sandström, M.; Jalilehvand, F.; Damian, E.; Fors, Y.; Gelius, U.; Jones, M.; Salomé, M. Sulfur accumulation in the timbers of King Henry VIII's warship Mary Rose: A pathway in the sulfur cycle of conservation concern. *Proc. Natl. Acad. Sci. U. S. A.* **2005**, *102* (40), 14165–14170.
- (40) Prietzel, J.; Botzaki, A.; Tyufekchieva, N.; Brettholle, M.; Thieme, J.; Klysubun, W. Sulfur speciation in soil by S K-edge XANES spectroscopy: comparison of spectral deconvolution and linear combination fitting. *Environ. Sci. Technol.* **2011**, *45* (7), 2878–2886.
- (41) Bohic, S.; Murphy, K.; Paulus, W.; Cloetens, P.; Salomé, M.; Susini, J.; Double, K. Intracellular chemical imaging of the developmental phases of human neuromelanin using synchrotron X-ray microspectroscopy. *Anal. Chem.* **2008**, *80* (24), 9557–9566.
- (42) Cuif, J.-P.; Dauphin, Y.; Doucet, J.; Salome, M.; Susini, J. XANES mapping of organic sulfate in three scleractinian coral skeletons. *Geochim. Cosmochim. Acta* **2003**, *67* (1), 75–83.
- (43) Hedley, M. J.; Stewart, J. W. B.; Chauhan, B. S. Changes in inorganic and organic soil phosphorus fractions induced by cultivation practices and by laboratory incubations. *Soil Sci. Soc. Am. J.* **1982**, *46* (5), 970–976.
- (44) Kahiluoto, H.; Kuisma, M.; Ketoja, E.; Salo, T.; Heikkinen, J. Phosphorus in manure and sewage sludge more recyclable than in soluble inorganic fertilizer. *Environ. Sci. Technol.* **2015**, *49* (4), 2115–2122.
- (45) Zhang, J.; Zuo, W.; Tian, Y.; Chen, L.; Yin, L.; Zhang, J. Sulfur transformation during microwave and conventional pyrolysis of sewage sludge. *Environ. Sci. Technol.* **2017**, *51* (1), 709–717.
- (46) Li, W.; Joshi, S. R.; Hou, G.; Burdige, D. J.; Sparks, D. L.; Jaisi, D. P. Characterizing phosphorus speciation of Chesapeake Bay sediments using chemical extraction, ³¹P NMR, and X-ray absorption fine structure spectroscopy. *Environ. Sci. Technol.* **2015**, *49* (1), 203–211.
- (47) Bender Koch, C.; Mørup, S. Identification of green rust in an ochre sludge. *Clay Miner.* **1991**, *26* (4), 577–582.
- (48) Rasmussen, H.; Nielsen, P. H. Iron reduction in activated sludge measured with different extraction techniques. *Water Res.* **1996**, *30* (3), 551–558.
- (49) Appels, L.; Baeyens, J.; Degrève, J.; Dewil, R. Principles and potential of the anaerobic digestion of waste-activated sludge. *Prog. Energy Combust. Sci.* **2008**, *34* (6), 755–781.
- (50) Foriel, J.; Philippot, P.; Susini, J.; Dumas, P.; Somogyi, A.; Salome, M.; Khodja, H.; Menez, B.; Fouquet, Y.; Moreira, D.; Lopez-Garcia, P. High-resolution imaging of sulfur oxidation states, trace elements, and organic molecules distribution in individual microfossils and contempo rary microbial filaments. *Geochim. Cosmochim. Acta* **2004**, *68* (7), 1561–1569.
- (51) Marti, N.; Bouzas, A.; Seco, A.; Ferrer, J. Struvite precipitation assessment in anaerobic digestion processes. *Chem. Eng. J.* **2008**, *141* (1), 67–74.

- (52) Tao, W.; Fattah, K. P.; Huchzermeier, M. P. Struvite recovery from anaerobically digested dairy manure: A review of application potential and hindrances. *J. Environ. Manage.* **2016**, *169*, 46–57.
- (53) Yan, H.; Shih, K. Effects of calcium and ferric ions on struvite precipitation: A new assessment based on quantitative X-ray diffraction analysis. *Water Res.* **2016**, *95*, 310–318.
- (54) Marti, N.; Pastor, L.; Bouzas, A.; Ferrer, J.; Seco, A. Phosphorus recovery by struvite crystallization in WWTPs: Influence of the sludge treatment line operation. *Water Res.* **2010**, *44* (7), 2371–2379.
- (55) Muryanto, S.; Bayuseno, A. P. Influence of Cu^{2+} and Zn^{2+} as additives on crystallization kinetics and morphology of struvite. *Powder Technol.* **2014**, *253*, 602–607.
- (56) Mamais, D.; Pitt, P. A.; Cheng, Y. W.; Loiacono, J.; Jenkins, D. Determination of ferric chloride dose to control struvite precipitation in anaerobic sludge digesters. *Water Environ. Res.* **1994**, *66* (7), 912–918.
- (57) Funke, A.; Ziegler, F. Hydrothermal carbonization of biomass: a summary and discussion of chemical mechanisms for process engineering. *Biofuels, Bioprod. Biorefin.* **2010**, *4* (2), 160–177.
- (58) Jiang, Y.; Yang, L.; Bohn, C. M.; Li, G.; Han, D.; Mosier, N. S.; Miller, J. T.; Kenttämä, H. I.; Abu-Omar, M. M. Speciation and kinetic study of iron promoted sugar conversion to 5-hydroxymethylfurfural (HMF) and levulinic acid (LA). *Org. Chem. Front.* **2015**, *2* (10), 1388–1396.
- (59) Lemos, V. P.; Costa, M. L. d.; Lemos, R. L.; Faria, M. S. G. d. Vivianite and siderite in lateritic iron crust: an example of bioreduction. *Quim. Nova* **2007**, *30*, 36–40.
- (60) O'Loughlin, E. J.; Boyanov, M. I.; Flynn, T. M.; Gorski, C. A.; Hofmann, S. M.; McCormick, M. L.; Scherer, M. M.; Kemner, K. M. Effects of bound phosphate on the bioreduction of lepidocrocite ($\gamma\text{-FeOOH}$) and maghemite ($\gamma\text{-Fe}_2\text{O}_3$) and formation of secondary minerals. *Environ. Sci. Technol.* **2013**, *47* (16), 9157–9166.
- (61) Rothe, M.; Kleeberg, A.; Hupfer, M. The occurrence, identification and environmental relevance of vivianite in waterlogged soils and aquatic sediments. *Earth-Sci. Rev.* **2016**, *158*, 51–64.
- (62) Shi, N.; Liu, Q.; He, X.; Wang, G.; Chen, N.; Peng, J.; Ma, L. Molecular structure and formation mechanism of hydrochar from hydrothermal carbonization of carbohydrates. *Energy Fuels* **2019**, *33* (10), 9904–9915.
- (63) Caccavo, F.; Frolund, B.; Van Ommen, K. F.; Nielsen, P. H. Deflocculation of activated sludge by the dissimilatory Fe(III)-reducing bacterium *Shewanella alga* BrY. *Appl. Environ. Microbiol.* **1996**, *62* (4), 1487–1490.
- (64) Lehtoranta, J.; Ekholm, P.; Pitkänen, H. Coastal Eutrophication Thresholds: A Matter of Sediment Microbial Processes. *Ambio* **2009**, *38* (6), 303–308.
- (65) Li, R.-h.; Cui, J.-l.; Li, X.-d.; Li, X.-y. Phosphorus removal and recovery from wastewater using Fe-dosing bioreactor and cofermentation: investigation by X-ray absorption near-edge structure spectroscopy. *Environ. Sci. Technol.* **2018**, *52* (24), 14119–14128.
- (66) Wild, D.; Kisliakova, A.; Siegrist, H. Prediction of recycle phosphorus loads from anaerobic digestion. *Water Res.* **1997**, *31* (9), 2300–2308.
- (67) Tagirov, B. R.; Suleimenov, O. M.; Seward, T. M. Zinc complexation in aqueous sulfide solutions: Determination of the stoichiometry and stability of complexes via $\text{ZnS}(\text{cr})$ solubility measurements at 100°C and 150bars. *Geochim. Cosmochim. Acta* **2007**, *71* (20), 4942–4953.
- (68) Dunnette, D. A.; Chynoweth, D. P.; Mancy, K. H. The source of hydrogen sulfide in anoxic sediment. *Water Res.* **1985**, *19* (7), 875–884.
- (69) Isa, Z.; Grusenmeyer, S.; Verstraete, W. Sulfate reduction relative to methane production in high-rate anaerobic digestion: technical aspects. *Appl. Environ. Microbiol.* **1986**, *51* (3), 572–579.
- (70) Yan, L.; Ye, J.; Zhang, P.; Xu, D.; Wu, Y.; Liu, J.; Zhang, H.; Fang, W.; Wang, B.; Zeng, G. Hydrogen sulfide formation control and microbial competition in batch anaerobic digestion of slaughterhouse wastewater sludge: Effect of initial sludge pH. *Bioresour. Technol.* **2018**, *259*, 67–74.
- (71) Wilkin, R. T.; Barnes, H. L. Pyrite formation by reactions of iron monosulfides with dissolved inorganic and organic sulfur species. *Geochim. Cosmochim. Acta* **1996**, *60* (21), 4167–4179.
- (72) Hurtgen, M. Anomalous enrichments of iron monosulfide in euxinic marine sediments and the role of H_2S in iron sulfide transformations; examples from Effingham Inlet, Orca Basin, and the Black Sea. *Am. J. Sci.* **1999**, *299*, 556–588.
- (73) Li, Y.; van Santen, R. A.; Weber, T. High-temperature FeS-FeS₂ solid-state transitions: Reactions of solid mackinawite with gaseous H_2S . *J. Solid State Chem.* **2008**, *181* (11), 3151–3162.
- (74) Legros, S.; Levard, C.; Marcato-Romain, C.-E.; Guisresse, M.; Doelsch, E. Anaerobic digestion alters copper and zinc speciation. *Environ. Sci. Technol.* **2017**, *51* (18), 10326–10334.
- (75) Wielinski, J.; Gogos, A.; Voegelín, A.; Müller, C.; Morgenroth, E.; Kaegi, R. Transformation of nanoscale and ionic Cu and Zn during the incineration of digested sewage sludge (biosolids). *Environ. Sci. Technol.* **2019**, *53* (20), 11704–11713.
- (76) Westerhoff, P.; Lee, S.; Yang, Y.; Gordon, G. W.; Hristovski, K.; Halden, R. U.; Herckes, P. Characterization, recovery opportunities, and valuation of metals in municipal sludges from U.S. wastewater treatment plants nationwide. *Environ. Sci. Technol.* **2015**, *49* (16), 9479–9488.
- (77) Peccia, J.; Westerhoff, P. We should expect more out of our sewage sludge. *Environ. Sci. Technol.* **2015**, *49* (14), 8271–8276.
- (78) Wang, S.; An, J.; Wan, Y.; Du, Q.; Wang, X.; Cheng, X.; Li, N. Phosphorus competition in bioinduced vivianite recovery from wastewater. *Environ. Sci. Technol.* **2018**, *52* (23), 13863–13870.
- (79) Liu, J.; Cheng, X.; Qi, X.; Li, N.; Tian, J.; Qiu, B.; Xu, K.; Qu, D. Recovery of phosphate from aqueous solutions via vivianite crystallization: Thermodynamics and influence of pH. *Chem. Eng. J.* **2018**, *349*, 37–46.
- (80) Tian, J.; Cheng, X.; Deng, S.; Liu, J.; Qiu, B.; Dang, Y.; Holmes, D. E.; Waite, T. D. Inducing in situ crystallization of vivianite in a UCT-MBR system for enhanced removal and possible recovery of phosphorus from sewage. *Environ. Sci. Technol.* **2019**, *53* (15), 9045–9053.
- (81) Muehe, E. M.; Morin, G.; Scheer, L.; Pape, P. L.; Esteve, I.; Daus, B.; Kappler, A. Arsenic(V) incorporation in vivianite during microbial reduction of arsenic(V)-bearing biogenic Fe(III) (oxyhydr)oxides. *Environ. Sci. Technol.* **2016**, *50* (5), 2281–2291.
- (82) Kocar, B. D.; Herbel, M. J.; Tufano, K. J.; Fendorf, S. Contrasting effects of dissimilatory iron(III) and arsenic(V) reduction on arsenic retention and transport. *Environ. Sci. Technol.* **2006**, *40* (21), 6715–6721.
- (83) Cheah, S.; Malone, S. C.; Feik, C. J. Speciation of sulfur in biochar produced from pyrolysis and gasification of oak and corn stover. *Environ. Sci. Technol.* **2014**, *48* (15), 8474–8480.
- (84) Churka Blum, S.; Lehmann, J.; Solomon, D.; Caires, E. F.; Alleoni, L. R. F. Sulfur forms in organic substrates affecting S mineralization in soil. *Geoderma* **2013**, *200–201*, 156–164.
- (85) Özverdi, A.; Erdem, M. Cu^{2+} , Cd^{2+} and Pb^{2+} adsorption from aqueous solutions by pyrite and synthetic iron sulphide. *J. Hazard. Mater.* **2006**, *137* (1), 626–632.